Turk J Phys
35 (2011) , 311 – 321.

doi:10.3906/fiz-1101-89

Stress-strain characteristics, dynamic recrystallization, grain growth, and melting point of the binary and ternary solder alloys

Shakib Moqbel Ali Mohammed ALSOWIDY and Mohammed Ali SHUKRI
Materials Science Laboratory, Physics Department Faculty of Science,
Sana'a University, Sana'a-YEMEN
e-mail: dralsowidy@yahoo.com

Received: 07.01.2011

Abstract

An advanced solder alloy, Pb-10wt%Sn-3wt%Zn, has been developed to improve the mechanical properties of the Pb-10wt%Sn based solders. Deformation behavior of Pb-10wt%Sn and Pb-10wt%Sn-3wt%Zn alloys was investigated in tension at strain rates from 0.005% to 0.25% s^{-1} in the temperature range 383–433 K. The stress-strain characteristics curves showed two deformation modes: (i) continuous work softening and fracture following a sharp stress in Pb-10wt%Sn, (ii) work hardening with steady-state flow and fracture just after yielding in Pb-10wt%Sn-3wt%Zn. In the work softening type, relatively coarse grains ranging from 30 to 60 μm are produced by dynamic recrystallization (DRX). In the work hardening with steady-state flow type, fine grains less than 10μm are developed by alloying with zinc. Adding Zn into the solder makes the microstructure finer and more uniform. Microstructural characterization using optical microscope analysis (OMA) were conducted to investigate the deformation behavior and cleared that the grain boundary sliding is the dominant mechanism observed in the Pb-10wt%Sn-3wt%Zn. The melting points have been determined using differential thermal analysis (DTA) and differential scanning calorimetry (DSC). These temperatures are 587 and 555 K for Pb-10wt%Sn and Pb-10wt%Sn-3wt%Zn, respectively. The addition of a small amount of Zn leads to reduce high temperature performance and melting point.

Key Words: Solder alloys, stress-strain curves, dynamic recrystallization, work softening, mechanical properties, grain growth, plastic deformation

1. Introduction

Pb-Sn alloys have emerged as a solder alloys for many structural and electronic applications due to its highly attractive properties, such as low melting temperature, wettability, good electrical conductivity, and low cost [1, 2]. Since the mechanical characterization of Pb-Sn alloys is of great complexity and strongly sensitive to the processing parameters, i.e. strain rate (SR) and deformation temperature (DT), it is important to clarify

its deformation modes. Technologically, these parameters have important implications: optimum temperature and optimum strain rate [3]. There is an obvious desire to lower the high temperature performance and shift the strain rates to higher levels.

A number of studies have been carried out to improve the flow behavior of Pb-Sn alloys by varying their structural state, in particular, the grain size, the grain boundaries area, and the addition of various alloying elements. The fact that the superplasticity is a grain size dependent phenomenon has led to extensive study on the grain size distribution, grain growth, grain aspect ratio, and phase homogeneity [4–13]. However, for achieving the optimum processing parameters in Pb-Sn alloys, alloying with some elements has been used. It was reported earlier [14] that the addition of Zn or Cd to Pb-Sn eutectic did not affect the material response during superplastic flow. Recent approaches by some authors [15] revealed that some contradictions about the effect of the third phase on the plastic deformation behavior of this alloy. It was reported that the Zn-addition in Pb-Sn eutectic improves the high temperature ductility, creep resistance [16] and electrical conductivity [17]. On the other hand, the Zn-rich phase enhances the phase transformation temperature [16]. Other authors have shown that the addition of Cd or Bi to Pb-Sn alloys increase the alloy response during plastic flow [18].

The first purpose of the present research is to develop a new Pb-Sn solder alloy by evaluation the effect of adding 3 wt% Zn on the characteristic curves for Pb-10wt%Sn at different DT and SR. The second purpose is to determine the mechanism of plastic deformation and evaluate any influence of Zn-addition on the microstructure and melting point for Pb-10wt%Sn.

2. Experimental procedures

The alloys Pb-10wt%Sn and Pb-10wt%Sn-3wt%Zn were prepared from Pb, Sn and Zn of 99.99% purity by vacuum melting. The ingots were cold drawn to wire samples of 0.8 mm in diameter and 30 mm length. The wires were then annealed at 400 K for 4 hours, then slowly cooled to room temperature at cooling rate of 0.02 K/s. This leads to obtain samples containing fully precipitated phases. After annealing, we noted that the microstructure consists of equiaxed and homogeneous grains with grain size of 50 μm and 10 μm for the binary and ternary alloys, respectively. The samples were tested using an Instron 4505 universal vertical tensile testing machine, with an error less than $\pm 3\%$. The tensile tests were performed at three different temperatures (383, 413, 433 K) and at four different strain rates (0.005%, .05%, 0.13%, 0.25% s^{-1}). The microstructure of the deformed specimens was investigated by using an optical microscope (OM). Using differential thermal analysis (DTA) and differential scanning calorimetry (DSC), the melting temperature has been determined for the two compositions.

3. Results and discussion

Figures 1 and 2 show series of typical true stress-strain of Pb-10wt%Sn and Pb-10wt%Sn-3wt%Zn alloys. Figure 1 shows the temperature dependence of a true stress-strain curves at a given initial strain rate. The strain rate dependence, at given deformation temperature, is shown in Figure 2. The curves in Figures 1 and 2 show different behavior for Pb-10wt%Sn and Pb-10wt%Sn-3wt%Zn specimens. For Pb-10wt%Sn, the curves are characterized by significant work softening and fracture following a sharp stress. For Pb-10wt%Sn-3wt%Zn, the curves are characterized by work hardening with steady state deformation and fracture just after smooth yielding. Generally, from these two figures, we see that the deformation temperature and strain rate have

obvious effects on the deformation behavior of the two alloys. Also, we can see that Pb-10wt%Sn-3wt%Zn has greater elongation than Pb-10wt%Sn.

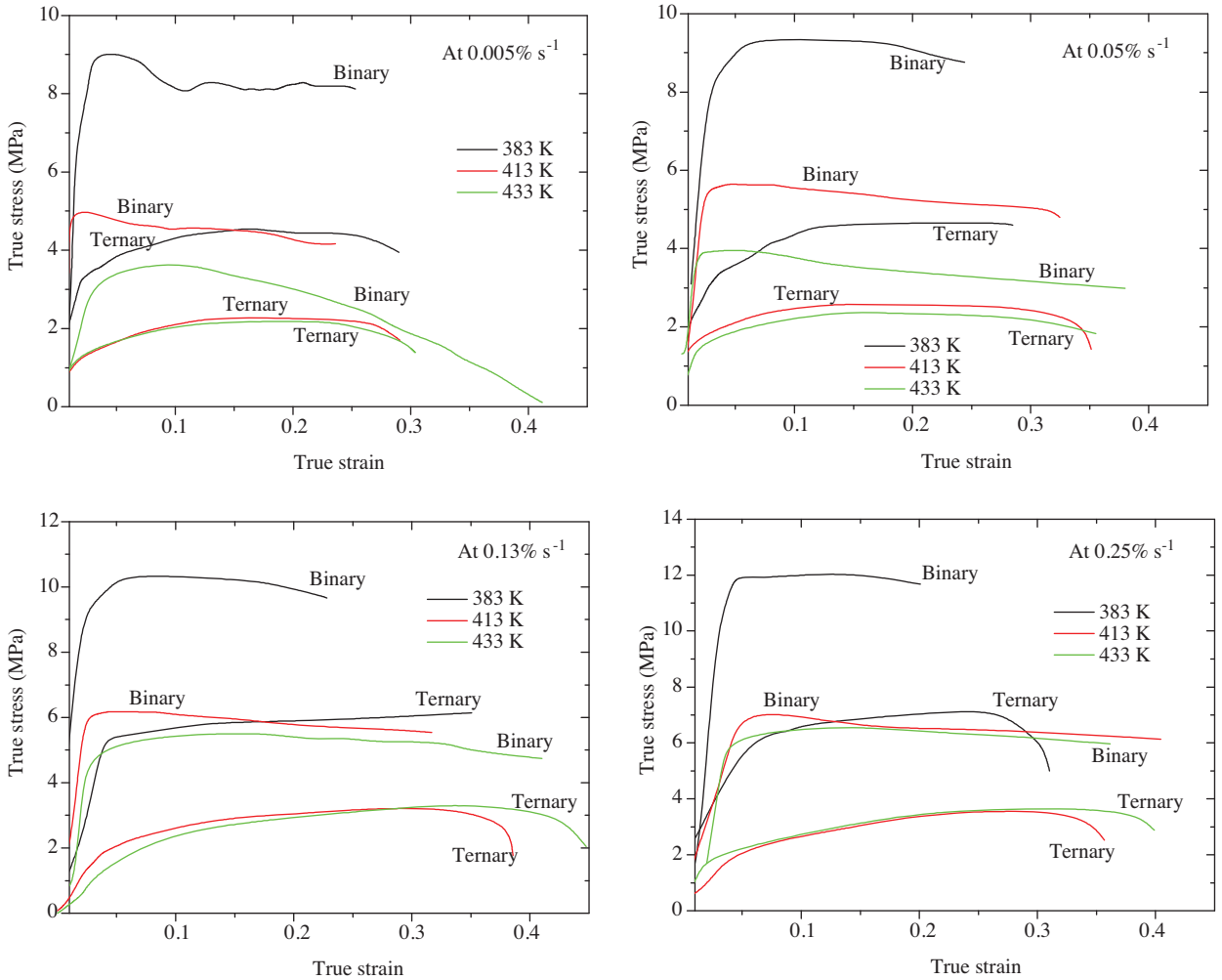

Figure 1. True stress-strain curves at different SR for Pb-10wt%Sn and Pb-10wt%Sn-3wt%Zn solder alloys.

Figure 3 shows clearly variation of the flow stress as a function of deformation temperature at different strain rates. The flow stress increases as deformation temperature decreases. All curves in this figure show that the flow stress in Pb-10wt%Sn is higher than that in Pb-10wt%Sn-3wt%Zn and the effect of Zn addition decreases with increasing temperature. The strain rate dependence of the flow stress is shown in Figure 4. The flow stress increases as the strain rate increases. At a given temperature, the flow stress is higher in binary than in ternary alloy.

From these results it becomes clear that the improvement of ductility of Pb-10wt%Sn-3wt%Zn is attributed to a number of contributing factors, including the presence of the Zn-content third phase.

In order to explain the observed deformation behavior of the binary and ternary alloys, microstructure analysis after deformation has been performed. Figures 5 and 6 show the grain structure of Pb-10wt%Sn and Pb-10wt%Sn-3wt%Zn alloys, which were pre-annealed at 400 K for 4 hours and deformed up to a strain of 0.3 at temperatures of 383, 413 and 433 K at an initial strain rate of 0.13% s^{-1}. From Figure 5, it can be seen

that the Pb-10wt%Sn had an equiaxed grain structure with an average grain size of 50 μm. Many new fine grains are nucleated in the structure. It is accepted that the formation of new fine grains and the equiaxed grain structure strongly suggest the occurrence of dynamic recrystallization (DRX) [9, 19].

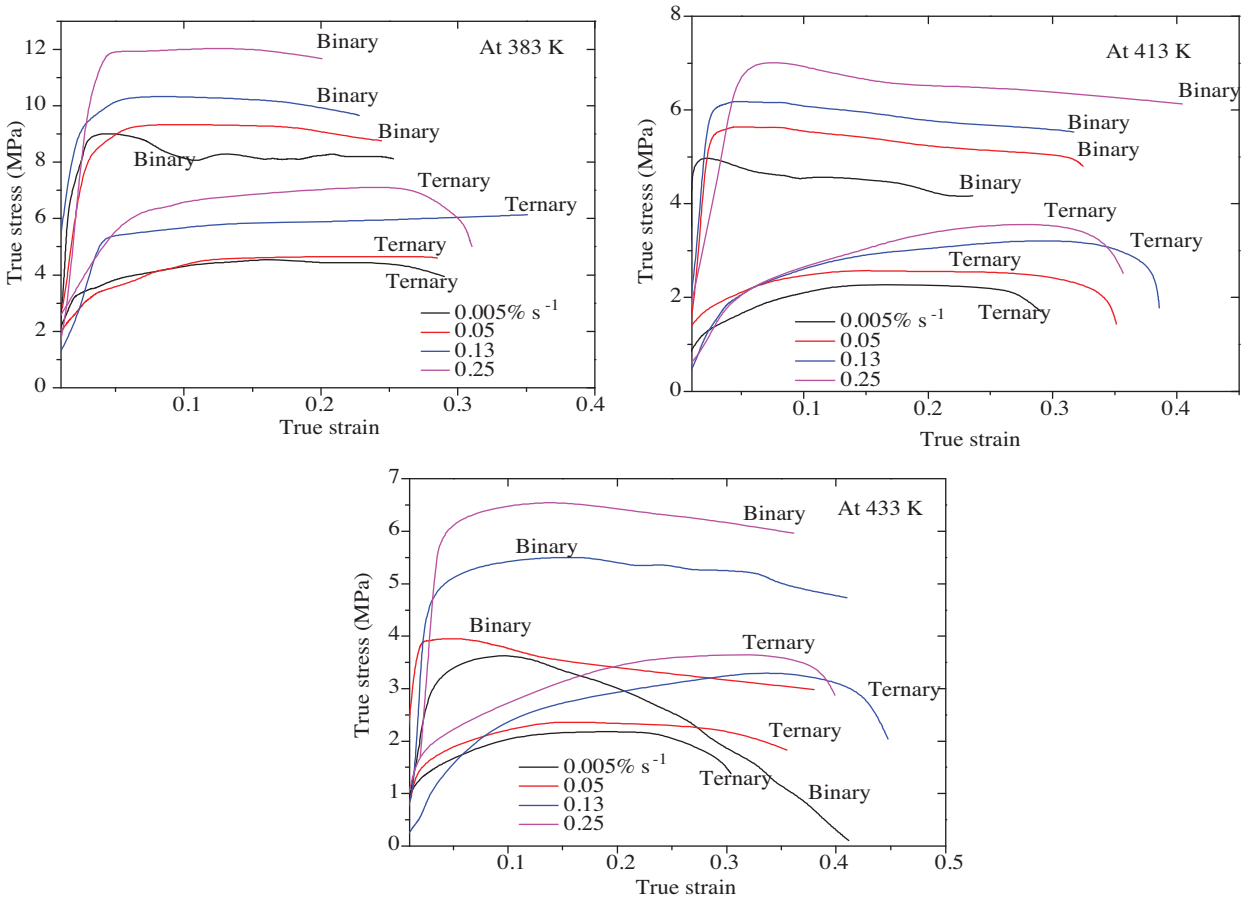

Figure 2. True stress-strain curves at different DT for Pb-10wt%Sn and Pb-10wt%Sn-3wt%Zn solder alloys.

At 433 K, the complete solution of Sn in α-phase has been obtained. The microstructure is fully recrystallized and the equiaxed phase is fully individualized and spheroidized. If we compare between Figures 5 and 6, we conclude that the content of Zn plays a vital role in grain refinement. We believe that non-dissolving Zn particles promote the coarse precipitates and therefore keep a refined grain size [16].

The grain refinement is attained with an average grain size of 10 μm. The superplastic behavior, grain size, and the multiplicity of types of interphase boundaries have been developed in Pb-65wt%Sn-3.4wt%Zn compared with Pb-65wt%Sn eutectic alloy as a result of Zn-addition [15]. Good combination of high ductility and low melting temperature by grain refinement has been shown in Pb-31.1wt%Sn-$_{3.4wt\%}$Zn alloy [20]. From these Figures (5, 6), high solubility of Sn in Pb rich phase is seen more pronounced in Figure 6. The grains are in an equiaxed array and there appears to be limited agglomerates of relatively fine and coarser grains. Close inspection showed that the grain boundaries are reasonably wavy and curved with cusps, finger like protuberances. All these observations are favorable for grain boundary sliding mechanism and suggest that the alloying element may be preferable for producing a thermal stable fine grain size [15]. The mechanical response here seems to depend on the change in the internal structure including a basic change in the grain size and

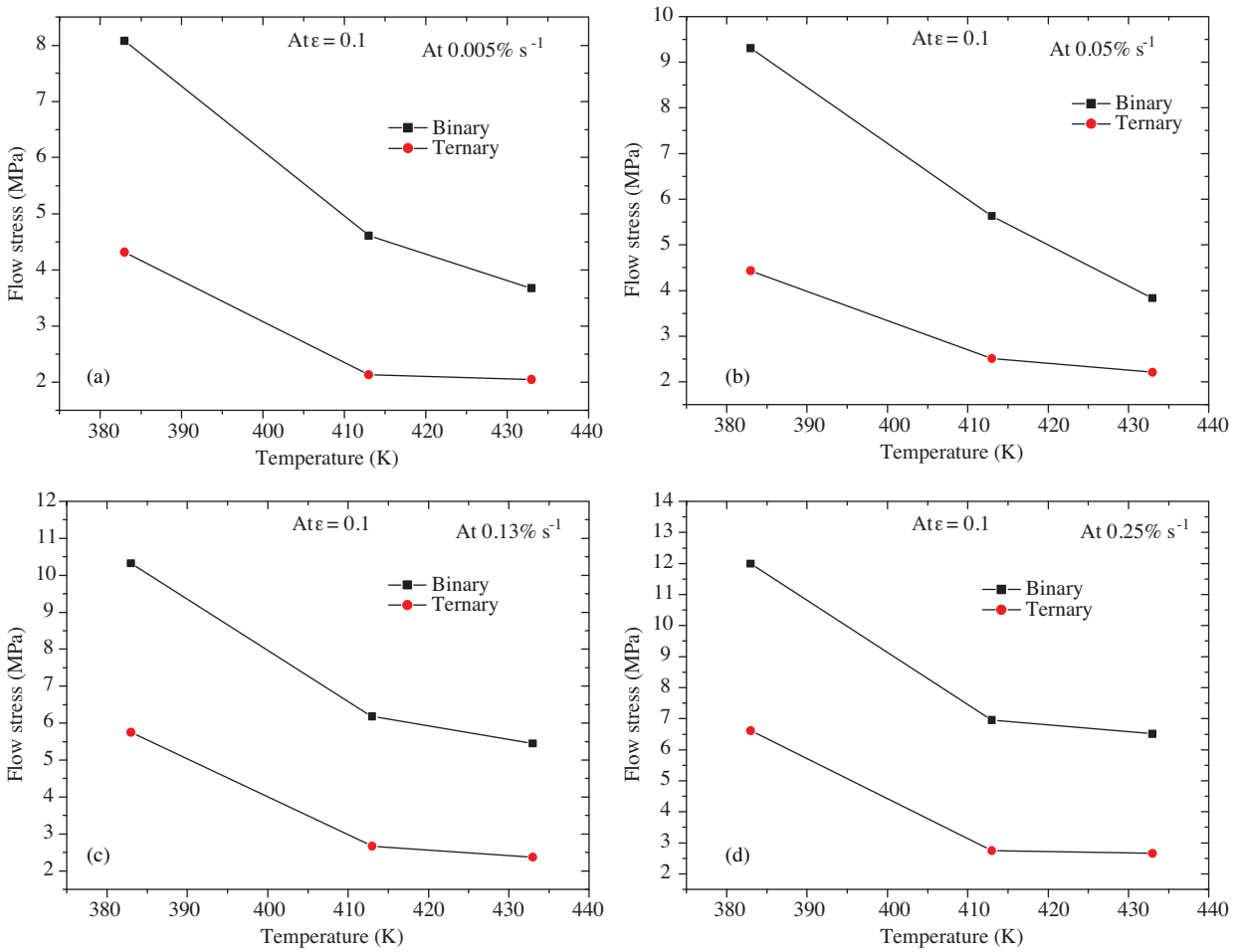

Figure 3. Variation of flow stress with deformation temperature at a constant strain rate of: (a) 0.005% s^{-1}, (b) 0.05% s^{-1}, (c) 0.13% s^{-1}, and (d) 0.25% s^{-1} for binary and ternary alloys.

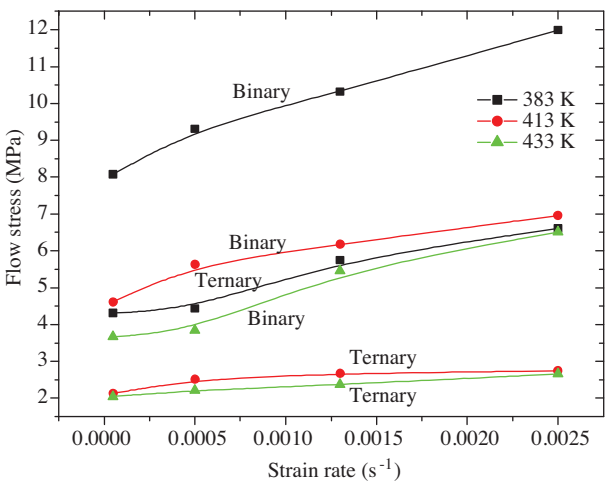

Figure 4. Variation of flow stress with stress rate at a constant deformation temperature.

grain boundaries at elevated temperatures and strain rates. Therefore, Zn particles act principally to refine and stabilize equiaxed grains of Sn-and Pb-rich solid solutions [16]. In contrast, it is suggested that the low degree of ductility and high tensile strength observed in Pb-10wt%Sn (Figures 1 and 2) can be explained by the coarsening process of the grains during deformation.

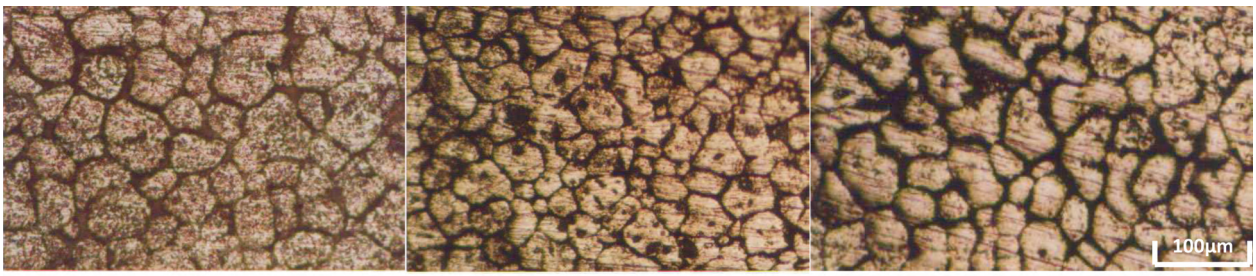

Figure 5. Metallographic micrographs of Pb-10wt%Sn samples pre-annealed at 450 K for 4 h and deformed up to a true strain of 0.3 at (a) 383 K, (b) 413 K, and (c) 433 K.

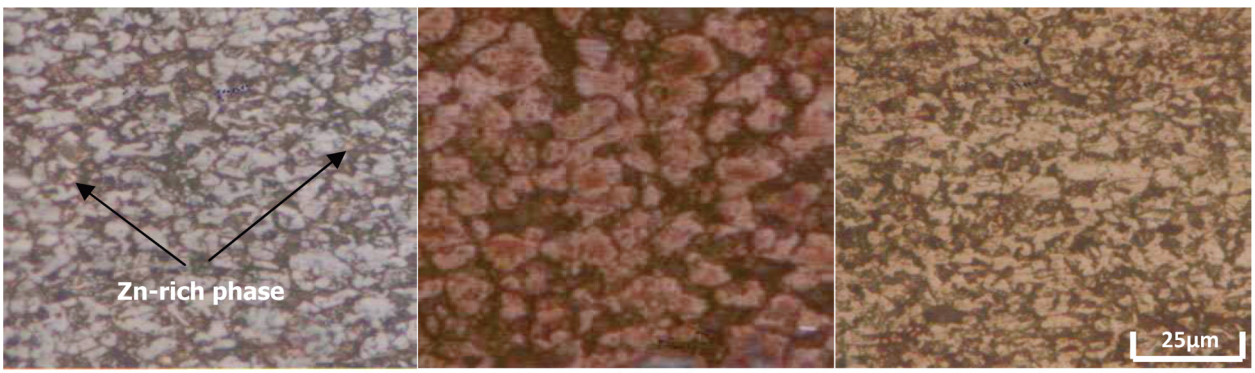

Figure 6. Metallographic micrographs of Pb-10wt%Sn-3wt%Zn samples pre-annealed at 450 K for 4 h and deformed up to a true strain of 0.3 at (a) 383 K, (b) 413 K, and (c) 433 K.

The activation energy at a constant strain rate has been determined using the following relation [14, 21]:

$$\dot{\varepsilon} = k \left(\frac{\sigma}{E}\right)^{1/m} \exp\left(-\frac{Q}{RT}\right), \tag{1}$$

where σ is the flow stress, k is a constant, E is the Young's modulus, R is the gas constant and m is the strain rate sensitivity parameter. Thus, Q can be determined by plotting $\ln\sigma$ against $1/T$, as shown in Figure 7. The values obtained of Q have been found to be 27 and 20 kJ/mole for the binary and ternary alloys, respectively. These values are the same as that reported for grain boundary diffusion of Sn in Pb-10wt%Sn alloy [22].

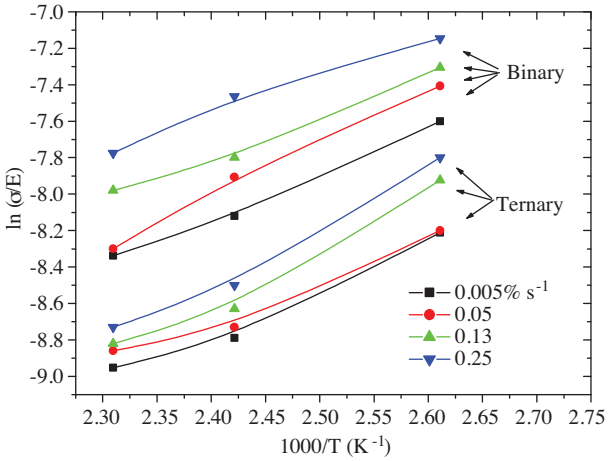

Figure 7. Reciprocal temperature dependence of elastic modulus compensated flow stress of Pb-10wt%Sn and Pb-10wt%Sn-3wt%Zn.

In order to identify the melting point, differential thermal analysis (DTA) has been carried out, as one can see in Figure 8. We can see the endothermal effects at 587 K and 555 K, for the binary and ternary compositions, respectively. This difference observed in the DTA analysis is attributed to the effect of the third phase (Zn-rich phase) which enhances the melting point of Pb-10wt%Sn-3wt%Zn solders. The verification of this reduction in melting temperature has been carried out using a differential scanning calorimeter (DSC), as shown in Figure 9. This reduction is attributed to the Zn-addition which accelerates the transformation from solidus to liquidus. From these analyses, we can conclude that the thermally activated has less time in Pb-10wt%Sn-3wt%Zn composition than in Pb-10wt%Sn composition. This is observed in lower flow stress for Pb-10wt%Sn-3wt%Zn in figures (3 and 4) and in lower activation energy observed in Figure 7.

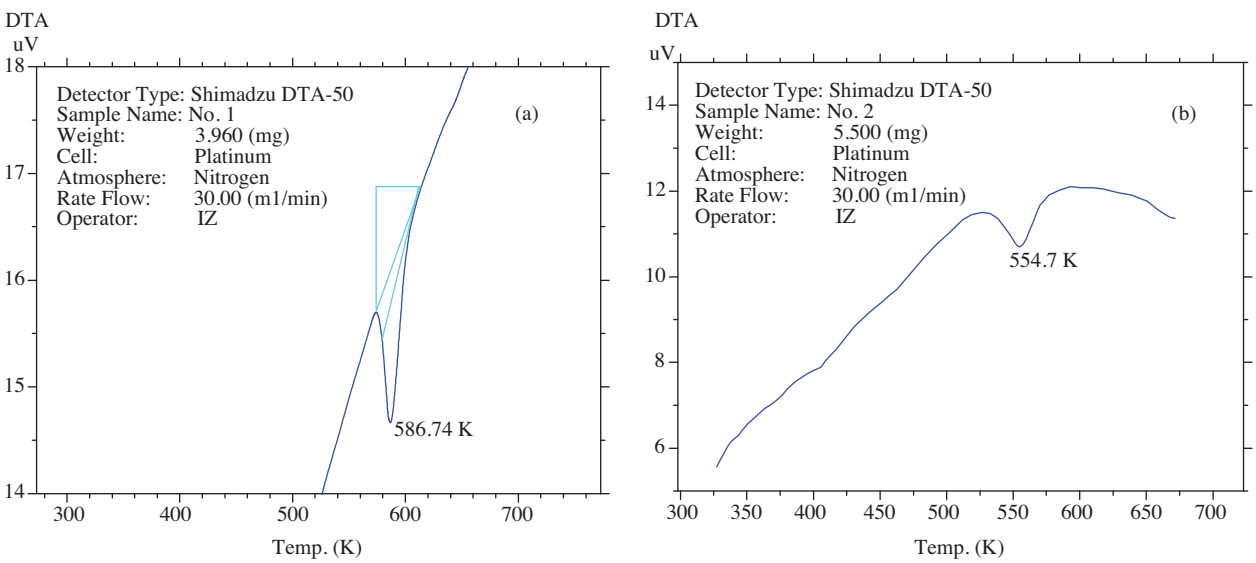

Figure 8. DTA analysis shows the melting point (T_m) for (a) Pb-10wt%Sn (b) Pb-10wt%Sn-3wt%Zn.

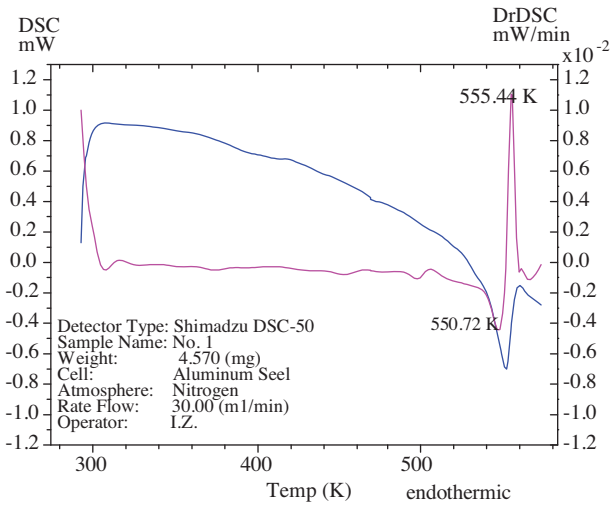

Figure 9. DSC analysis shows the melting point for Pb-10wt%Sn-3wt%Zn alloy.

The stress-strain curves of Pb-Sn solders depend on the mechanical characterization of these alloys. These curves exhibit two different modes of deformation, work softening and work hardening with steady-state for the Pb-10wt%Sn and Pb-10wt%Sn-3wt%Zn compositions, respectively. The work softening after a high stress peak is often observed in many Pb-Sn alloys. This work softening has been interpreted in occurrence of dynamic recrystallization (DRX) followed by grain boundary sliding (GBS) between fine DRX grains less than 20 μm [9]. Since the grains of Pb-10wt%Sn are larger than 20 μm (see Figure 5), this interpretation is not consistent. The grain size is too large to cause grain boundary sliding before many dislocations glide within grains and the deformation proceeds dominantly by climb accompanied with DRX. Similar observation has been reported by Kim et al. [19].

It is not clearly understood what deformation mechanism which is the most appropriate for the experimental data obtained. However, some models may be consistent with this data [15, 23]. The model of Ball and Hutchison is the most appropriate for explain the data obtained. This model involves movement of groups of four grains (Figure 10(a)). Protrusions on the boundaries of certain grains obstruct easy sliding between groups of grains. Therefore, the local stress caused by sliding of the interfaces makes the dislocations traverse the grains and pile up against the opposite boundaries until the back stress prevents further sliding. Dislocation climbing into and along the grain boundaries makes further sliding possible.

The above mechanism is more pronounced for Pb-10wt%Sn alloy as we can observe in Figure 10(b). The movement of group of grains along the GBS plane can produce dislocations which pile-up against the opposite boundaries of the blocking grain. This process can produce local stresses at the grain boundaries necessary for grain cleavage and fracture of the blocking grain.

On the other hand, grain growth during deformation of Pb-10wt%Sn will create concentrated regions of high stress at grain boundaries leading to fracture under high flow stresses. The cleavage and fracture of the blocking grain is required to relieve the high stress concentration and attain small grain size.

The steady-state flow of Pb-10wt%Sn-3wt%Zn is indicative of more plasticity properties of this alloy. The elongation of the ternary alloy is closely related to the fine grain size and the relation between the flow stress and grain size is quite similar to that of Pb-Sn-Zn type alloys [15, 16].

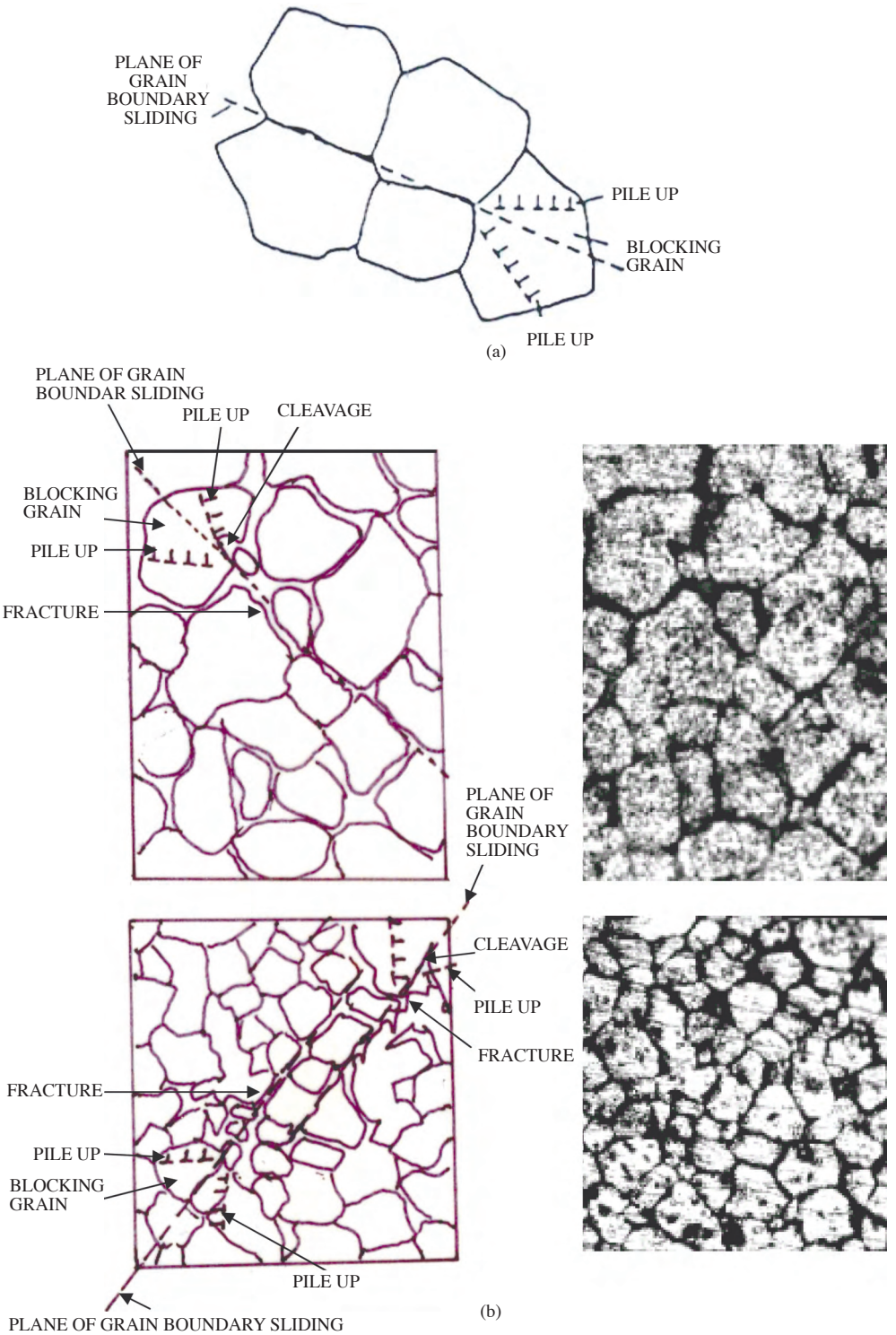

Figure 10. **(a)** Schematic representation of the model of Ball and Hutchison [22] showing sliding between a group of grains. **(b)** A schematic representation of Pb-10Sn samples show the plane of grain boundary sliding between a group of grains (see Figure 5 a and b).

4. Conclusions

- Observation concerning stress level and melting temperature are technologically important for industrial development of lead-based solder alloys processes, since stress variations on the order of three can be observed with Zn-containing alloys.
- Stress during tensile appears to be a very sensitive parameter of the morphology and processing parameters of Pb-Sn alloys.
- The microstructure of the Pb-10wt%Sn-3wt%Zn solder is sensitive to the Zn addition.
- The initial microstructure of the Pb-10wt%Sn-3wt%Zn is finer and uniform than that of the Pb-10wt%Sn solder.
- The melting temperature for the Pb-10wt%Sn-3wt%Zn is less than that for the Pb-10wt%Sn composition.
- The apparent activation energies of the Pb-10wt%Sn-3wt%Zn and Pb-10wt%Sn were 20 kJ/mole and 27 kJ/mole, respectively.

References

[1] X. Chen, L. Zhang, M. Sakane and H. Nose, *Key Eng. Mat.*, **297-300,** (2005), 905.

[2] C. Kanchanomai, Y. Miyashita and Y. Mutoh, *Int. J. of Fat.*, **24,** (2002), 671.

[3] R. Mishra and A. Mukherjee, *J. Mat. Sci.*, **35,** (2000), 147.

[4] M. Ruggiero and J. Rutter, *Mat. Sci. Tech.,* **15,** (1999), 1110.

[5] R. Yadava and K. Padmanabhan, *J. Mat. Sci.,* **17,** (1982), 2435.

[6] M. Butt and M. Nadeem, *J. Mat. Sci. Lett.*, **20,** (2001), 763.

[7] G. Li and Y. Chan, *Mat. Sci. Eng.,* **B57,** (1999), 116.

[8] J. Seconde and M. Suery, *J. Mat. Sci.,* **19,** (1984), 3995.

[9] S. Wong, P. Hodgson and P. Thomson, *Mat. Sci. Tech.,* **15,** (1999), 689.

[10] J. Kim, D. Li and C. Lee, *Mat. Sci. Tech.,* **14,** (1998), 676.

[11] C. Briant, *Mat. Sci. Tech.*, **17,** (2001), 1317.

[12] B. Bai, H. Yang, N. Chen and A. Mukherjee, *Mat. Sci. Tech.,* **17,** (2001), 269.

[13] A. El-Daly and A. Abdel-Daiem, *phys. stat. sol. (a)*, **197**, (2003), 56.

[14] M. Moles and G. Davies, *Met. Sci. Sep.,* (1976), 314.

[15] A. El-Daly, A. Abdel-Daiem and M. Yousef, *Mat. Chem. phys.,* **74,** (2002), 43.

[16] A. El-Daly, A. Abdel-Daiem, E. El-Saadani, A. Abdel-Rahman and S. Mohammed, *Mat. Chem. phys.*, **83,** (2004), 96.

[17] A. El-Daly, A. Abdel-Daiem and M. Yousef, *Mat. Chem. phys.,* **78,** (2002), 73.

[18] A. Mohamed, M. El-Gazaly and E. El-Saadani, *Egypt. J. Sol.,* **18,** (1995), 197.

[19] W. Kim, S. Hanada and T. Sakai, *Mat. Sci. Eng.,* **A248,** (1998), 78.

[20] A. El-Daly, *phys. stat. sol. (a)*, **200**, (2003), 333.

[21] V. Balasubrahmanyam and Y. Prasad, *Mat. Sci. Tech.*, **17,** (2001), 1222.

[22] M. El-Sayed, F. Abdel-Salam and R. Abdel-Hasseb, *phys. stat. sol. (a),* **147,** (1995), 401.

[23] A. Mukherjee, *Annual Rev. Mat. Sci.,* **9,** (1979), 191.